Hindawi
Shock and Vibration
Volume 2021, Article ID 4370981, 16 pages
https://doi.org/10.1155/2021/4370981

Research Article

Analysis on Multimode Nonlinear Resonance of an Asymmetric Rolling Bearing Rotor with the Application of a Squeeze Film Damper

Chen Huizheng,[1] Zhong Shun,[2] Lu Zhenyong,[1] Chen Yushu,[2] and Liu Xiyu[1]

[1]*Institute of Dynamics and Control Science, Shandong Normal University, Ji'nan 250014, China*
[2]*Department of Mechanics and Key Laboratory of Nonlinear Dynamics and Control, Tianjin University, Tianjin 300072, China*

Correspondence should be addressed to Zhong Shun; shunzhong@tju.edu.cn

Received 26 July 2021; Accepted 31 August 2021; Published 21 September 2021

Academic Editor: Athanasios Chasalevris

This paper takes an asymmetric ball bearing supported rotor system with the application of a squeeze film damper (SFD) subjected by unbalanced force and parametric excitation (varying compliance) as the research object. The dynamical behaviours of the system in multimode resonance regions with the application of the SFD are investigated. In each resonance region, the amplitude-frequency curves are obtained under conditions of with SFD and without SFD, as well as the spectrum analysis of the solutions. Through the results and comparisons of two cases, the damping effects of the SFD for each kind of resonance are illustrated. Meanwhile, the parameters of the ball bearing are also considered and analyzed with the application of SFD; the changing of the parameters of bearing would lead to the change in nonlinear dynamical behaviours. The findings would provide a theoretical basis for further vibration suppression and parameters' optimization of ball bearing supported rotor structure.

1. Introduction

Because of the high working rotating speed, the rotor structures in aeroengines [1–3] are supported by rolling bearings [4–8]. Rolling bearings are a type of main support for aeroengines and are a key source of vibration (parametric excitation) in rotor-bearing systems, which create a demand for vibration analysis and diagnostic techniques under various operating conditions [9]. Studying the nonlinear behaviour of the system and identifying the influence of rolling element bearing parameters on the nonlinear behaviours of the rotor system will help to reasonably avoid system instability, increase the operating life, and improve the efficiency of mechanical equipment [10]. Thus, the rolling bearing supported rotor systems have drawn many research interests [11–17].

The bearing introduced nonlinearity which makes the research complex. For a nonlinear system, not only the main resonances of each order could occur but also the nonlinear resonances, which are more complicated and wider in range, will appear. The early research of the nonlinear phenomena in rolling bearings could be traced back to 80s. Fukuta et al. [18] found that ball bearing systems have nonlinear dynamic behaviours such as superharmonic, subharmonic, quasi-periodic, and chaos-like solutions. Mevel and Guyader [19, 20] considered that the system entered chaos through a period-doubling bifurcation and explained the relationship between chaos motion and the contact failure. The resonance types of a multi-degree-of-freedom rolling bearing-rotor system mainly contain (1) prime resonances of each order, that is, the resonance when the external frequency is equal to the natural frequency of the system, (2) superharmonic or subharmonic resonances, which are caused by the nonlinear relationship between the excitation and response in the nonlinear system, (3) quasi-periodic

resonances, and (4) combination resonances. Therefore, it is necessary to add damping structures to suppress the unexpected resonances. The squeeze film damper (SFD) is one of the dampers usually used in aeroengines.

As a support structure with damping function, the SFD has been widely used in aeroengines due to its small size and light weight and has even become a standard configuration in the design. Many researchers focused on the design of SFD and its application effects to the rotor system. Zhang et al. [21] presented a multiobjective optimal design method for a squeeze film damper with centering spring. The proposed method was able to obtain the optimal design parameters for a flexible rotor system. Shaik and Dutta [22, 23] proposed a close form solution to find the nonlinear tuning parameters of symmetric or asymmetric rotor-squeeze film damper system. They also dealt with the development of a close form solution to find the stability of flexible symmetric horizontal rigid and tuned flexible rotor mounted on hydrodynamic bearing with squeeze film damper system. Zheng et al. [24] proposed a controllable clearance squeeze film damper which used hydraulic pressure to adjust the radial clearance and established a corresponding test rig. Fan and Behdinan [25] investigated the effect of a circumferential central groove on an open-ended squeeze film damper analytically. Shin et al. [26] treated the unconventional application of the SFD for the mitigation of Morton effect-induced vibration. Ma et al. [27] emphasized the comparative analysis of the influence of SFD on the nonlinear dynamic behaviour of the dual-rotor system supported by rolling bearings. Chen et al. [28] investigated dynamic characteristics of the rotor system mounted on aircraft during maneuvering flights. Iacobellis et al. [29] designed and built SFD-rotor test rig to study the effect of SFD oil supply pressure, oil temperature, oil inlet feed number/orientation, unbalance, and seals on the response of a Jeffcott rotor. Li et al. [30] manufactured and tested a pair of 3.5 inch SFD bearings to validate a new squeeze film damper bearing design.

From the existing work, the complexity of the response of rolling bearings, the damping effect of squeeze film dampers, and the nonlinear stiffness imposed on the nonlinear damping system all need further study. To further investigate the dynamical behaviours and achieve better or desired performances of the rotor systems with SFD, so as to provide a theoretical basis for the corresponding vibration reduction design strategy, the design of the parameters of the SFD need focused attention. Therefore, this work will focus on the dynamic analysis of the ball bearing supported rotor system with the application of the SFD and their parameter analysis. The paper is organized as follows. In Section 2, a ball bearing-rotor system model with SFD installed is established. The detailed modeling processes of the bearing and oil force are described. In Section 3, the dynamic analysis of the ball bearing-rotor system with or without SFD is conducted. In Section 4, parameters' analysis of the ball bearing act on the dynamic behaviour is given out. Section 5 discusses the comparison results, and Section 6 concludes the whole work.

2. Modeling of the Rotor System with SFD

Figure 1 shows a schematic diagram of a Jeffcott rotor system supported by ball bearings. The left and right ends have different ball bearing support schemes, respectively, as the left end is connected to the foundation with a spring and the right end is directly connected to the foundation without elastic structure. So, the degree of freedom of the outer ring of the left bearing must be considered while the right one can be ignored.

Considering the gravity, unbalanced force, gyroscopic effect, and bearing force, the dynamic model of the rotor support structure shown in Figure 1 can be established into form

$$\mathbf{M}\ddot{\mathbf{X}} + (\mathbf{C} + \Omega\mathbf{G})\dot{\mathbf{X}} + \mathbf{K}\mathbf{X} + \mathbf{F}_n = \mathbf{F}_u + \mathbf{F}_g, \tag{1}$$

where $\mathbf{X} = [\mathbf{x}, \mathbf{y}, \theta_x, \theta_y, x_a, y_a, x_b, y_b, x_o, y_o]^T$ is displacement coordinate vector, in which x and y are disc displacements along the x-axis and y-axis, respectively, θ_x and θ_y are disc rotating angles along the x-axis and y-axis, respectively, x_a and y_a represent the displacements of the equivalent mass at the left end journal, x_b and y_b represent the displacements of the equivalent mass at the right end, and x_o and y_o represent the displacements of the outer ring of the bearing mounted at the left. **M**, **C**, **G**, and **K** are corresponding mass matrix, damping matrix, gyro matrix, and stiffness matrix, whose expressions can be found in appendix.

$\mathbf{F}_n = [0, 0, 0, 0, F_{bx1}, F_{by1}, F_{bx2}, F_{by2}, F_{cx} - F_{bx1}, F_{cy} - F_{by1}]^T$ is the bearing force vector, $\mathbf{F}_u = [m\delta\Omega^2 \cos \Omega t, m\delta\Omega^2 \sin \Omega t, 0, 0, 0, 0, 0, 0, 0, 0]^T$ is unbalanced force vector, and $\mathbf{F}_g = [0, -mg, 0, 0, 0, -m_a g, 0, -m_b g, 0, -m_o g]^T$ is gravity vector. Ω is rotating frequency which determines the frequency of the unbalanced force.

The bearing force model adopted in this work is a two-degree-of-freedom ball bearing model, including nonlinear Hertzian contact force, clearance, and variable stiffness characteristics. Assuming that the initial positions of the bearing balls at both ends are the same, the position of the ball i at time t can be expressed as

$$\theta_i = \frac{2\pi(i-1)}{N_b} + \Omega_c t, \tag{2}$$

where N_b is the number of the rolling balls and $\Omega_c = r_i/(r_i + r_o) \cdot \Omega$, in which, r_i is the radius of the inner ring and r_o is the radius of the outer ring.

Then, the bearing force of the left end can be expressed as

$$\begin{bmatrix} F_{bx1} \\ F_{by1} \end{bmatrix} = C_b \sum_{i=1}^{N_b} \left(\delta_{1i} H[\delta_{1i}]\right)^{3/2} \begin{bmatrix} \cos\theta_{1i} \\ \sin\theta_{1i} \end{bmatrix}, \tag{3}$$

where $\delta_{1i} = (x_a - x_o)\cos\theta_i + (y_a - y_o)\sin\theta_i - \delta_0$, C_b is the Hertz contact stiffness, $H[\cdot]$ is Heaviside function, and δ_0 is the radial clearance of bearing.

Meanwhile, the bearing force of the right end can be expressed as

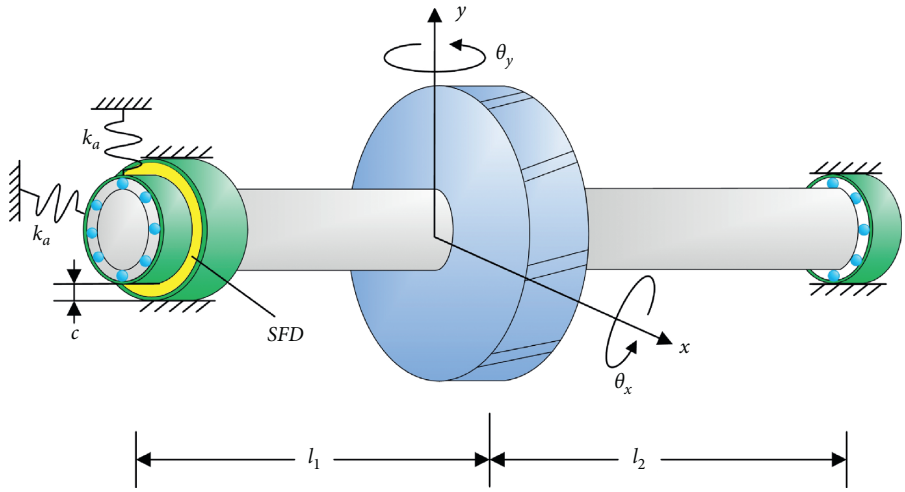

Figure 1: Schematic diagram of a Jeffcott rotor.

$$\begin{bmatrix} F_{bx2} \\ F_{by2} \end{bmatrix} = C_b \sum_{i=1}^{N_b} \left(\delta_{2i} H[\delta_{2i}]\right)^{3/2} \begin{bmatrix} \cos\theta_{2i} \\ \sin\theta_{2i} \end{bmatrix}, \tag{4}$$

where $\delta_{2i} = x_b \cos\theta_i + y_b \sin\theta_i - \delta_0$.

The oil film force adopts a short bearing approximate model, and the expression is

$$\begin{aligned} F_{cx} &= F_r \frac{x_o}{r} - F_\tau \frac{y_o}{r}, \\ F_{cy} &= F_r \frac{y_o}{r} + F_\tau \frac{x_o}{r}, \end{aligned} \tag{5}$$

where

$$\begin{aligned} F_r &= \frac{\mu R L^3}{c l^3 \left(I_3^{02}\dot{r} + I_3^{11} r\dot{\psi}\right)}, \\ F_\tau &= \frac{\mu R L^3}{c l^3 \left(I_3^{11}\dot{r} + I_3^{20} r\dot{\psi}\right)}, \end{aligned} \tag{6}$$

where r is the radial displacement of the journal center at each support, and its expression is

$$r = \sqrt{x_o^2 + y_o^2}, \tag{7}$$

ψ is the whirl angle of each journal, and the expression is

$$\psi = \arctan\left(\frac{y_o}{x_o}\right), \tag{8}$$

μ is the viscosity coefficient of the lubricating oil at each journal, R is the radius of each journal bearing, L is the length of each damper.

$$I_n^{lm} = \int_{\theta_1}^{\theta_2} \frac{\sin^l\theta \cos^m\theta}{(1 + r\cos\theta/cl)^3} \mathrm{d}\theta, \tag{9}$$

is the Sommerfeld coefficient.

Defining the dimensionless time as $\tau = \Omega t$ and dimensionless displacement vector $\mathbf{Q} = \mathbf{EX}$, in which $E = 1/c\mathrm{diag}(1, 1, l, l, 1, 1, 1, 1, 1, 1)$; equation (1) can be transformed into

$$Q'' + (\overline{\mathbf{C}} + \overline{\mathbf{G}})Q' + \overline{\mathbf{KQ}} + \overline{\mathbf{F}}_n = \overline{\mathbf{F}}_u + \overline{\mathbf{F}}_g, \tag{10}$$

where $\overline{\mathbf{C}} = 1/\Omega \mathbf{EM}^{-1}\mathbf{CE}^{-1}$ is dimensionless damping matrix, $\overline{\mathbf{G}} = EM^{-1}\mathbf{GE}^{-1}$ is the dimensionless gyro matrix, $\overline{\mathbf{K}} = 1/\Omega^2 \mathbf{EM}^{-1}\mathbf{KE}^{-1}$ is the dimensionless stiffness matrix, $\overline{\mathbf{F}}_n = 1/\Omega^2 \mathbf{EM}^{-1}\mathbf{F}_n$ is the dimensionless bearing force vector, $\overline{\mathbf{F}}_u = 1/\Omega^2 \mathbf{EM}^{-1}\mathbf{F}_u$ is the dimensionless unbalanced force vector, and $\overline{\mathbf{F}}_g = 1/\Omega^2 \mathbf{EM}^{-1}\mathbf{F}_g$ is the dimensionless gravity vector. The superscript prime denotes the derivative with respect of dimensionless time. The values of the system parameters are listed in Table 1. It should be mentioned that, as the stiffness is time varying, the mean of the response valves are used here as

$$\begin{aligned} k_{xx} &= \frac{1}{N}\sum_{i=1}^{N} \frac{\partial F_x}{\partial x}(i\Delta\tau), \\ k_{yy} &= \frac{1}{N}\sum_{i=1}^{N} \frac{\partial F_y}{\partial y}(i\Delta\tau), \end{aligned} \tag{11}$$

where $N = T/\Delta\tau$ is the number of discrete points.

3. Dynamical Analysis with the Application of SFD

3.1. Main Resonance and Quasi-Periodic Motion. In this section, the amplitude-frequency characteristics of the structure are going to be investigated. A dimensionless excitation frequency defined as $\lambda = \Omega/300$ is introduced for further analysis. Figure 2 gives the amplitude-frequency curves of the responses of the disc in horizontal direction with different parameters described by the governing equations of 1 with or without SFD. Obviously, the SFD plays a significant role in reducing the amplitude in the first-order main resonance region of the system. Accordingly, the resonance band as well as jump-bistable region reduces with the application of the SFD.

Table 1: The values of the parameters.

Parameters	Values
Rotor parameters	
m	120 kg
m_a	12 kg
m_b	18 kg
k_{rr}	7.4×10^7 N/m
$k_{r\varphi}$ and $k_{\varphi r}$	2.77×10^7 N/m
$k_{\varphi\varphi}$	6.15×10^7 N/m
k_a	1.0×10^7 N/m
c_1	266 Ns/m
c_2 and c_3	99.6 Ns/m
c_4	221 Ns/m
l_1	0.8 m
l_2	1.25 m
J_d	2.5 kg·m^2
J_p	2.5 kg·m^2
δ	1.67×10^{-6} m
Bearing parameters	
r_i	39.6 mm
r_o	70.4 mm
m_o	0.965 kg
C_b	1.0×10^9 N/m$^{3/2}$

Figure 3 gives the amplitude-frequency curves in the frequency region which is from $\lambda = 1.5$ to $\lambda = 7.0$. The blue dashed line in Figure 3 indicates the amplitude-frequency curve when the SFD is not applied. Quasi-periodic solutions exist in the third-order resonance region of $\lambda = 5.96$ and the region from $\lambda = 2.0$ to $\lambda = 4.0$, which covers the second-order main resonance region. The thick solid line indicates the amplitude-frequency response after adding the SFD. Although being suppressed, the quasi-periodic solutions which are located on the third-order resonance region still have large amplitudes. The spectrum is shown in Figures 3(b) and 3(c), where the quasi-periodic response of $\lambda = 6.09$ not only corresponds to the first-order resonance $\lambda_f = 0.93$ but also to the second-order resonance of $\lambda_f = 2.68$, by introducing a definition of an absolute quasi-periodic frequency $\lambda_f = \lambda \cdot \omega$, where ω is the frequency of the response.

In the quasi-periodic motion, from $\lambda = 2.0$ to $\lambda = 4.0$, the damping effect of the SFD is significant. The large and continuous quasiperiodic motion is reduced to a relatively independent area with a small amplitude. For the horizontal direction of the disc, there is a relatively smooth area between the first-order and third-order resonance regions. In addition, in the second-order resonance region ($\lambda = 2.6$ to 2.76), a cross structure with soft and hard characteristics coexisting appears.

Figure 4 gives amplitude-frequency curves of response of the left-end journal in horizontal direction in the same frequency region as Figure 3(a). There are obvious resonance peaks in this region, as well as some jump phenomena. The frequency spectrum analysis is performed around the second-order main resonance ($\lambda = 2.67$). The leftmost resonant peak in Figure 4 is near $\lambda = 1.88$, and the corresponding frequency component is shown in Figure 5(a). The dominant frequency is 1/2 VC frequency. Figure 5(b) corresponds to the second-order resonance frequency at $\lambda = 2.67$. It can be seen that the second-order resonance area is periodic motion and there is jump behaviour. In addition, there are obvious jump phenomena in the region from $\lambda = 5.25$ to 5.6. Taking the two solutions at $\lambda = 5.42$, the spectrums are shown in Figures 5(c) and 5(d). The run-down curve is a periodic motion, while the run-up curve has subharmonic frequency component. Therefore, the resonance peak is the subharmonic resonance peak of the second-order natural frequency. Compared with the results under the condition of no SFD, subharmonic resonance of the second-order frequency also occurs, indicating that this is a phenomenon caused by the nonlinearity of the bearing.

Corresponding to the peaks of the amplitude-frequency curves at $\lambda = 2.05$, $\lambda = 2.86$, $\lambda = 2.97$, and $\lambda = 3.58$ in Figure 4, the spectrums are shown in Figure 6. Besides the excitation frequency and the VC frequency, there are unconventional frequency components. These components are quasi-periodic motions, and the corresponding absolute quasi-periodic frequencies are (a) $\lambda_f = 2.677$, (b) $\lambda_f = 2.688$, (c) $\lambda_f = 2.682$, and (d) $\lambda_f = 0.918$. The first three relate to the second-order main resonance.

3.2. VC Frequency Resonance and Its 1/2 Subresonance. Figure 7 shows the amplitude-frequency curves during the VC frequency resonance region with different numbers of balls when the SFD is implemented. With the same damper configuration, the vertical resonance peak no longer shows the jump phenomenon of the soft stiffness characteristics as indicated in [10], but the horizontal direction still maintains the cross structure of the coexisting of the soft and the hard stiffness characteristics. This means that the strong coupling between two directions is not easy to dissipate the vibration energy. The SFD has no obvious effect on the amplitude and resonance zone. This is because, under the small amplitude vibration case, the nonlinear damping characteristics is not easy to exert its vibration. Meanwhile, different numbers of balls does not lead the vibration characteristics change, compared to no SFD cases.

In Figure 8, the influence of the SFD on the 1/2 subharmonic VC frequency resonance is illustrated by the reduction or disappearance of the hysteresis areas. When $N_b = 13$, the 1/2 subharmonic VC frequency resonance disappears. Basically, the SFD does not change the subharmonic resonance range of the original system. In addition, compared to [10], when $N_b = 8$, the quasi-period with large amplitude near $\lambda = 6.78$ disappears after adding the SFD. That means the 1/2 subharmonic resonance of the VC frequency can be eliminated by adjusting the number of balls. In case that the quasi-period exists, the SFD could improve the jump phenomenon in the subharmonic resonance region of the VC frequency, but its amplitude suppression effect is limited.

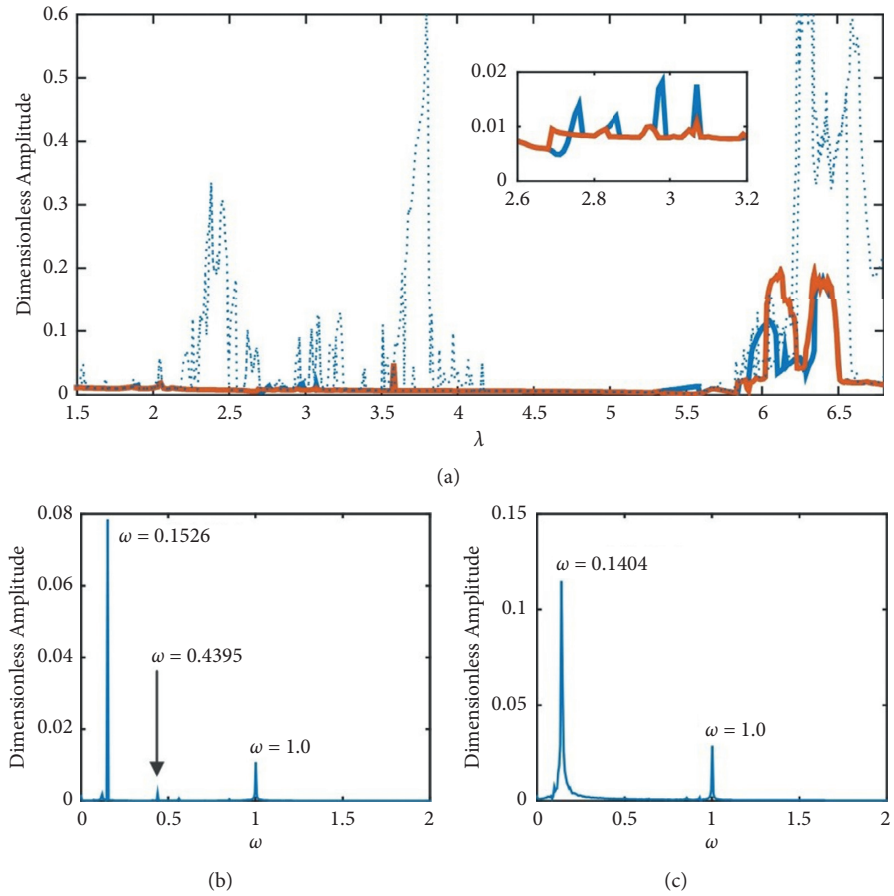

Figure 2: The amplitude-frequency curves in first-order primary resonance region.

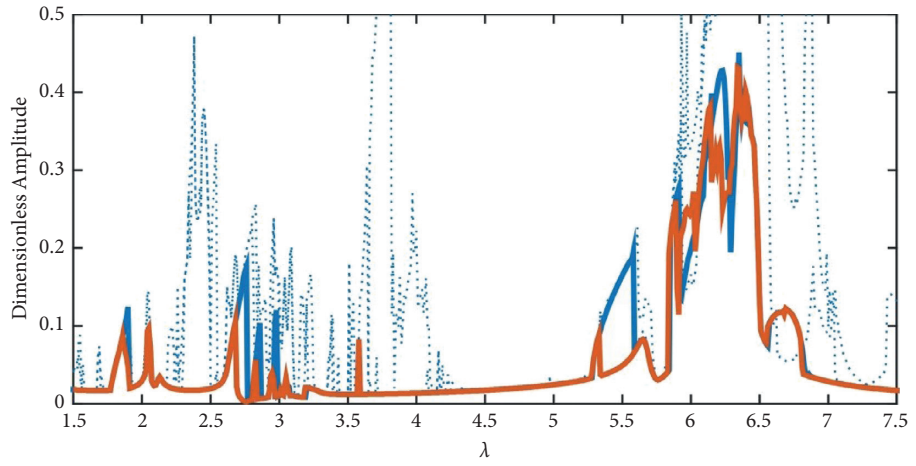

Figure 3: The amplitude-frequency curves and spectrum of responses of disc in horizontal direction when $N_b = 8$. (a) Amplitude-frequency curves, (b) spectrum at $\lambda = 6.09$, and (c) spectrum at $\lambda = 6.38$ (blue dot line means no SFD installed, solid line means the SFD is mounted, blue means run-up process, and brown means run-down process).

4. Parameter Analysis of the Ball Bearing with the Application of SFD

When $N_b = 9$, the amplitude-frequency curve of the disc in horizontal direction is shown in Figure 9(a). The second-order resonance shows the cross structure which means the coexistence of soft and hard stiffnesses. The spectrum of the run-up curve contains double frequency component, while the run-down curve has only periodic-1 response, as shown in Figures 9(b) and 9(c). The results are same as those when

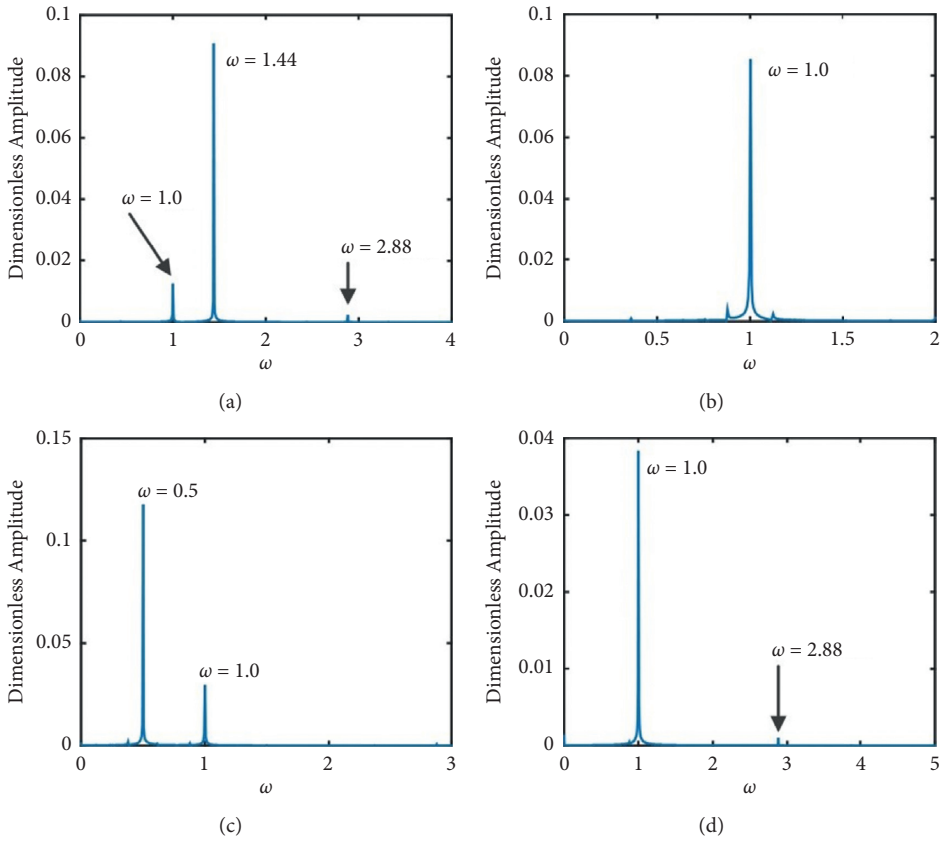

Figure 4: The amplitude-frequency curves of responses of left-end journal in horizontal direction when $N_b = 8$ (blue dot line means no SFD installed, solid line means the SFD is mounted, blue means run-up process, and brown means run-down process).

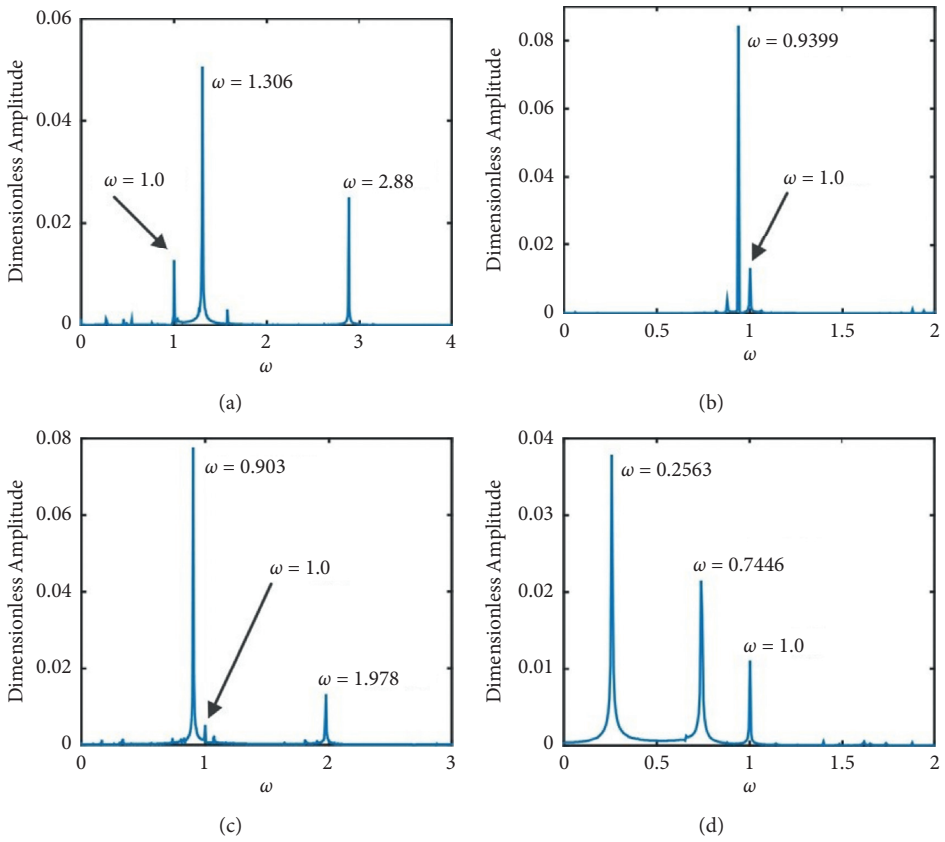

Figure 5: Spectrums of the responses at (a) $\lambda = 1.88$, (b) $\lambda = 2.67$, (c) $\lambda = 5.42$ (run-up), and (d) $\lambda = 5.42$ (run-down) when $N_b = 8$.

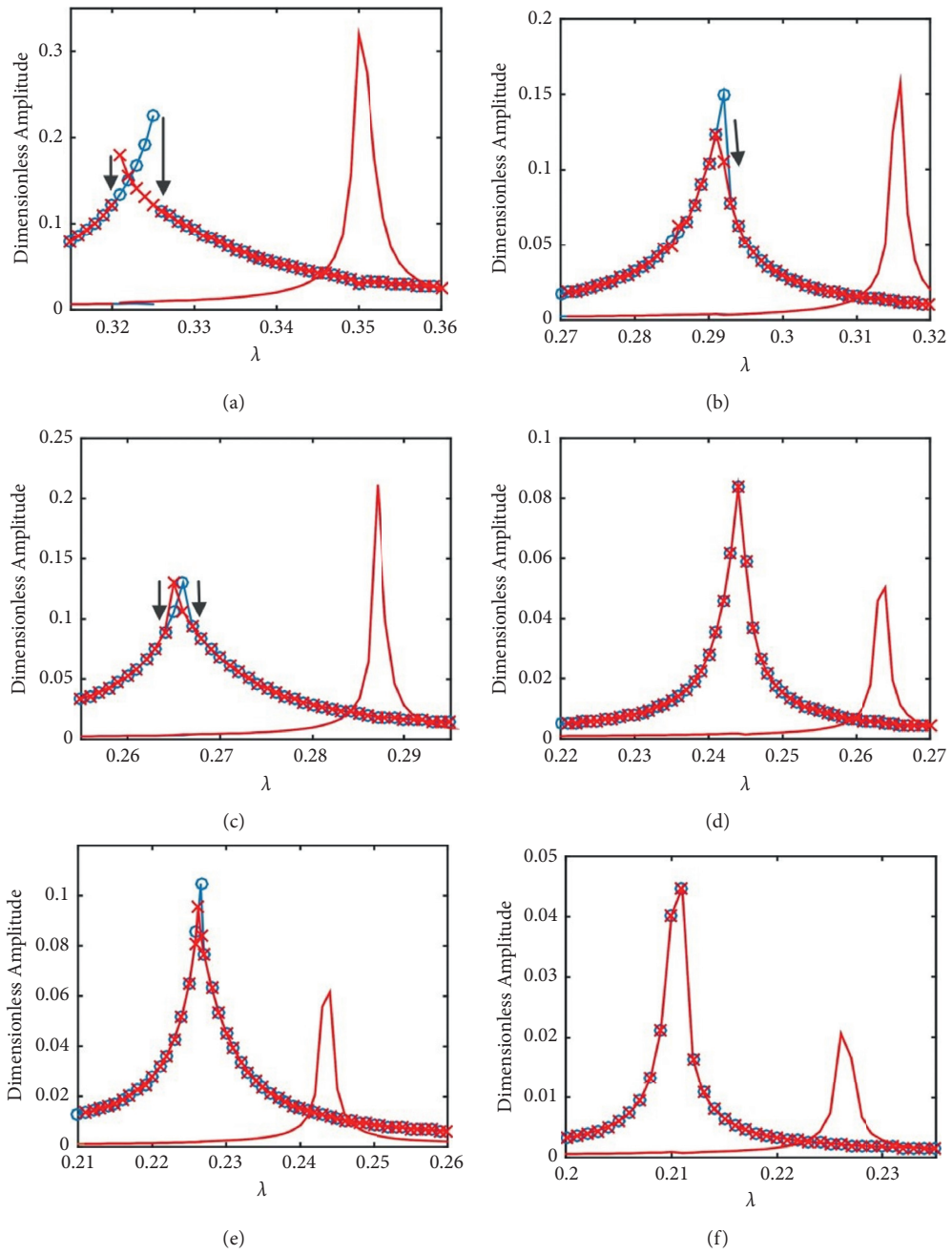

Figure 6: Spectrums of the responses at (a) $\lambda = 2.05$, (b) $\lambda = 2.86$, (c) $\lambda = 2.97$, and (d) $\lambda = 3.58$ when $N_b = 8$.

no SFD is mounted. Thus, the nonlinear characteristics are introduced by ball bearing support structure and do not been suppressed by the SFD.

It is noting that, in Figure 9(a), there is a jump region between $\lambda = 5.51$ and 5.64. In the region, corresponding to $\lambda = 5.6$, the frequency spectrum of run-up and run-down curves are shown in Figures 10(a) and 10(b). The adjacent region of $\lambda = 5.7$ to 6.0 also merges jump behaviour. The spectrums of run-up and run-down curves at $\lambda = 5.85$ are shown in Figures 10(c) and 10(d). Furthermore, taking the response at $\lambda = 5.69$, the frequency spectrum shows periodic motion (Figure 10(e)). Therefore, it can be concluded that the two regions are independent to each other. The former is the 1/2 subharmonic vibration caused by the second-order natural frequency region. And, the latter is the 1/2 subharmonic vibration caused by the third-order main resonance of the system. From $\lambda = 6.0$ to 6.3, period-1 and its 1/2 subharmonic components coexist. Then, the quasiperiodic motion merges, which is shown in Figure 10(f). Corresponding to the frequency $\lambda_f = 0.910$, it locates on the first-order main resonance frequency region. Meanwhile, other quasi-periodic responses' frequencies could be calculated as $\lambda_f = 2.754$, $\lambda_f = 0.927$, and $\lambda_f = 0.943$, which correspond to the first and second natural frequencies of the system, respectively.

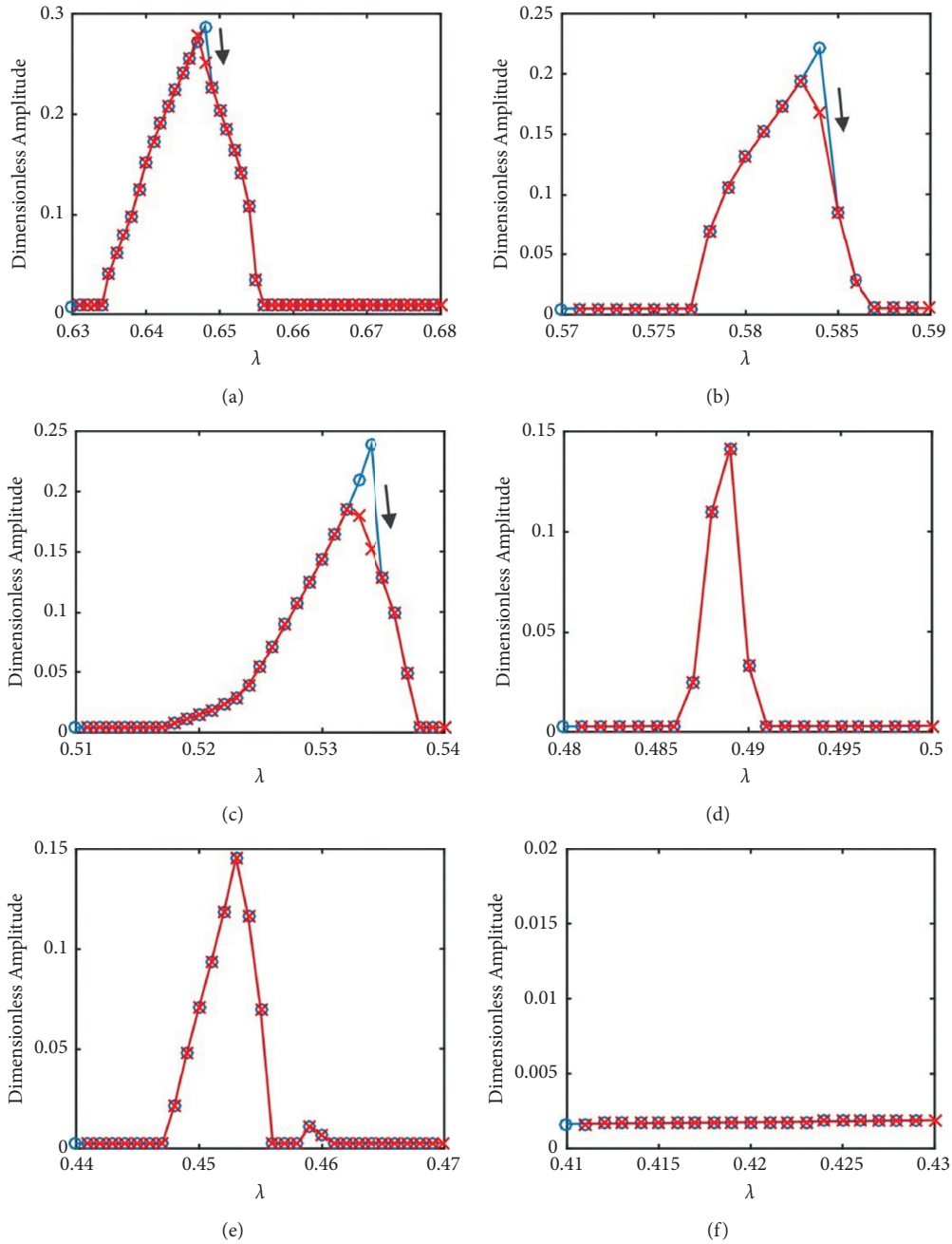

Figure 7: The amplitude-frequency curves in VC frequency resonance region, where ° indicates run-up and × indicates run-down.

Figure 11 shows the amplitude-frequency curve of the disc in horizontal direction when $N_b = 10$. Its main characteristics, including crossover characteristic in the second-order resonance, the subharmonic resonance of the VC frequency, the subharmonic response of the third-order main frequency, and the quasi-periodic motion corresponding to the third-order main resonance, are the same as those of the case of $N_b = 9$. However, in this case, the subharmonic resonance region corresponding to the second-order resonance has been merged into the subharmonic response region of the third-order main resonance. In addition, near $\lambda = 5.18$, the frequencies of run-up and run-down curves are all quasi-periodic, which is not consistent with other cases. It can be seen that this is due to the coupling effect of the SFD and the bearing. The stability condition at this frequency is destroyed, which leads the instability interval expanding. The quasi-periodic regions and frequencies are $\lambda = 1.74$ and $\lambda_f = 2.84$, $\lambda = 3.39$ and $\lambda_f = 0.952$, $\lambda = 3.78$ and $\lambda_f = 0.946$, and $\lambda = 5.18$ and $\lambda_f = 0.948$.

Figure 12 shows the amplitude-frequency curves of the disc in horizontal direction with N_b varies from 11 to 13. As the number of balls increases, the jump phenomenon of the second-order main resonance weakens and disappears, and

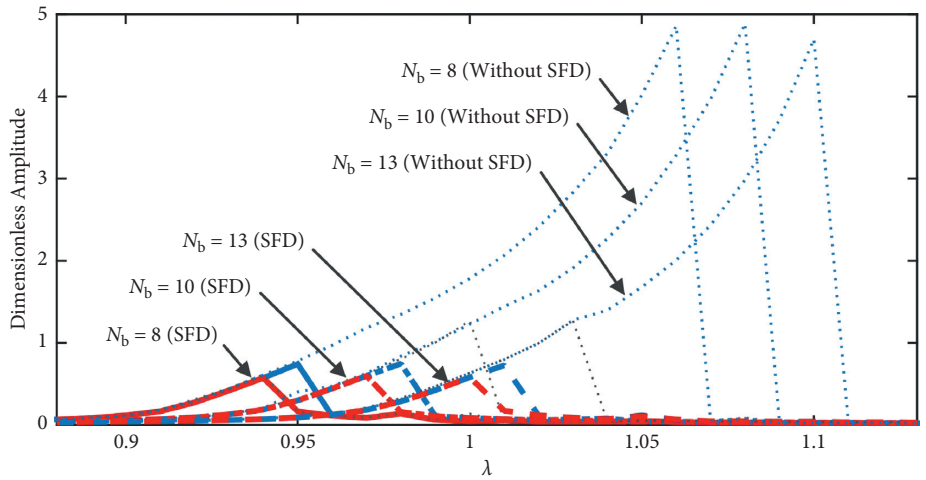

FIGURE 8: The amplitude-frequency curves in subharmonic VC frequency resonance region, where ∘ indicates run-up and × indicates run-down.

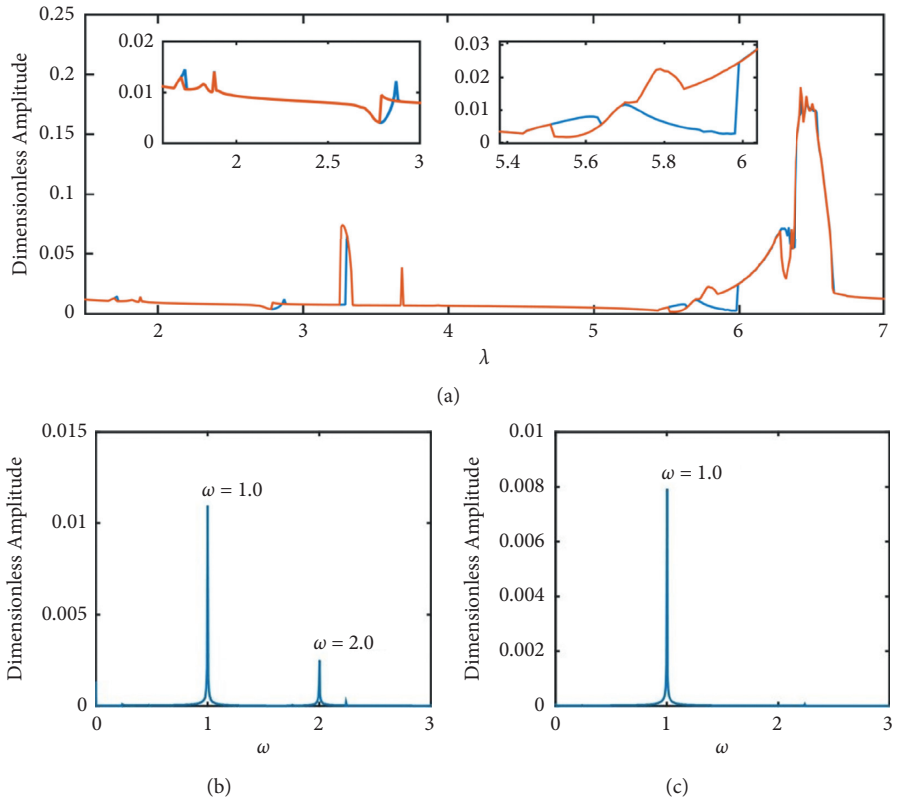

FIGURE 9: The amplitude-frequency curves and spectrums of responses of disc in horizontal direction when $N_b = 9$. (a) The amplitude-frequency curves, (b) $\lambda = 2.87$ (run-up), and (c) $\lambda = 2.87$ (run-down) (blue line means run-up process and brown line means run-down process).

the corresponding quasi-periodic area also decreases and disappears. In general, compared with the system with even number of balls, the quasi-period areas are less than those when the number of balls is odd. The quasiperiodic areas and corresponding frequencies of the system are listed in Table 2.

For horizontal comparisons, Figure 13 plots the amplitude-frequency curve of the left end journal in horizontal direction when $N_b = 9$ to 13. The change process of the quasi-periodic motion frequencies with the increase of the number of balls can be clearly seen.

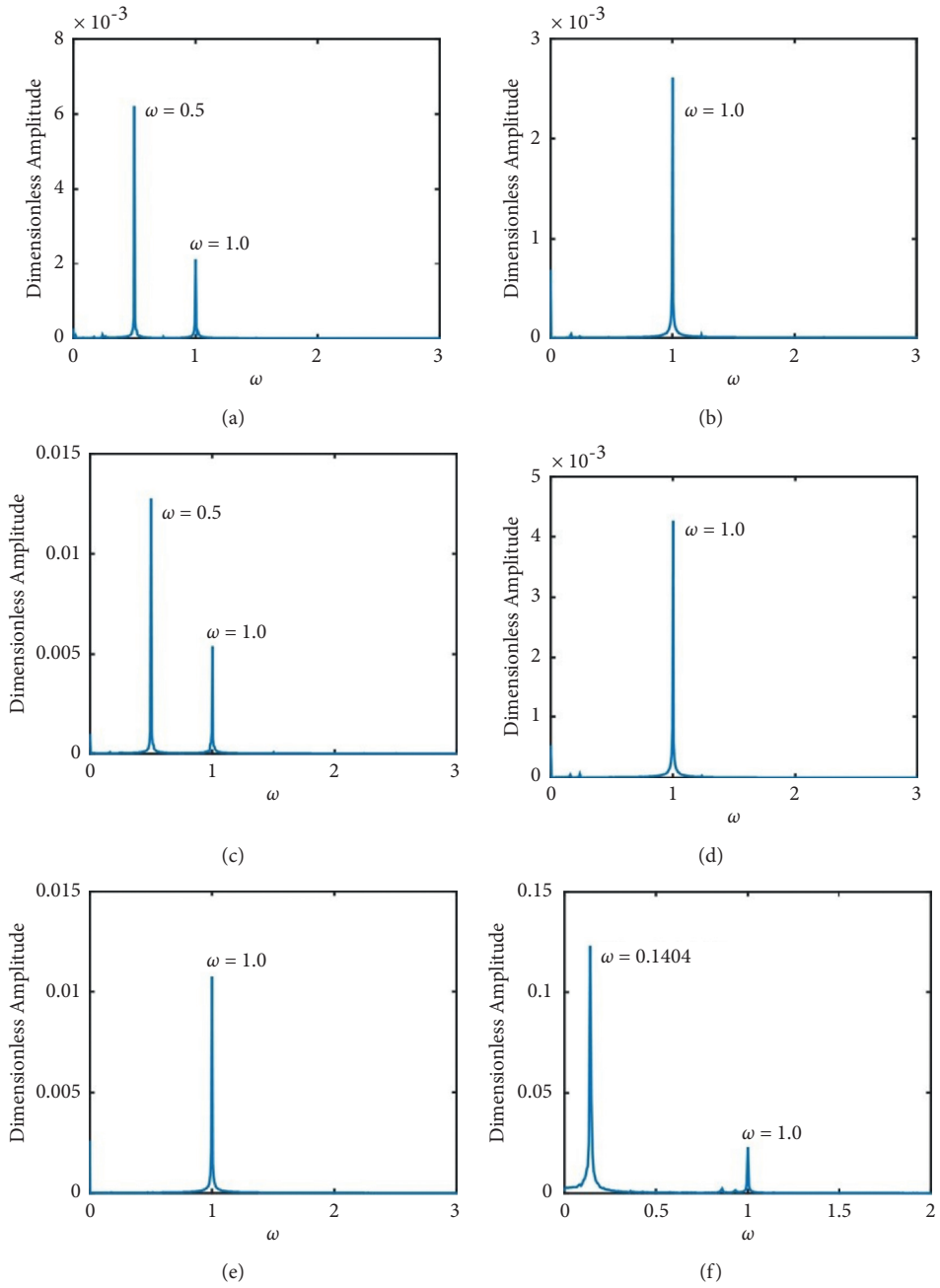

Figure 10: Spectrums of the responses at (a) $\lambda = 5.6$ (run-up), (b) $\lambda = 5.6$ (run-down), (c) $\lambda = 5.85$ (run-up), (d) $\lambda = 5.85$ (run-down), (e) $\lambda = 5.69$, and (f) $\lambda = 6.48$ when $N_b = 9$.

5. Discussion

Through the previous analysis, we can see that, in the area whose corresponding frequency is smaller than first-order natural frequency which is normalized to 1, as the number of balls increases, the VC frequency peak generally decreases, and the stability of the system with odd-numbered balls is slightly better than that with even-numbered balls. The subresonance of VC frequency corresponds to the first-order natural frequency which is suppressed. In this way, with the application of the SFD, the main resonance peaks of each order can be reduced. The peak and area of the quasi-period motion can also be reduced. In this process, the SFD and the bearing have a coupling effect in certain intervals, which will increase the instability region. Therefore, it is necessary to adjust the damper parameters to further control the vibration of the system because the outer ring of the bearing could offset against the effects of gravity and bearing forces. Meanwhile, to increase the damping by reducing the gap is likely to cause rubbing at the journal. Therefore, it is much more safe to adjust the length or viscosity.

Figure 14 shows the amplitude-frequency curves of the disc and the left journal in horizontal direction when $N_b = 13$ and $L = 16$ mm. The first-order main resonance peak no

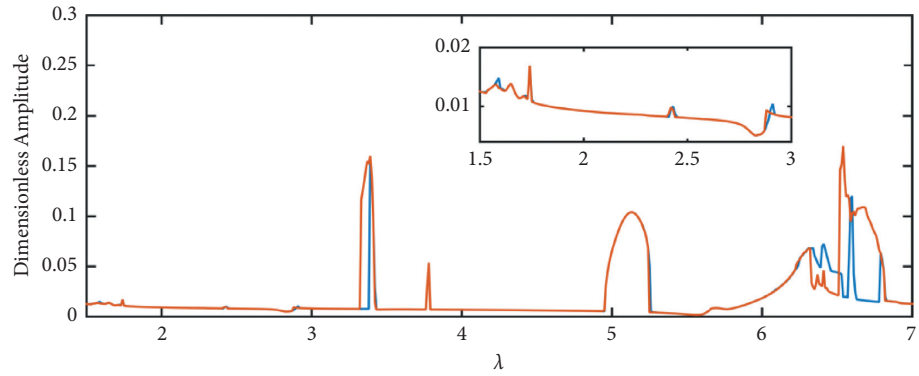

FIGURE 11: The amplitude-frequency curves of responses of disc in horizontal direction when $N_b = 10$ (blue line means run-up process and brown line means run-down process).

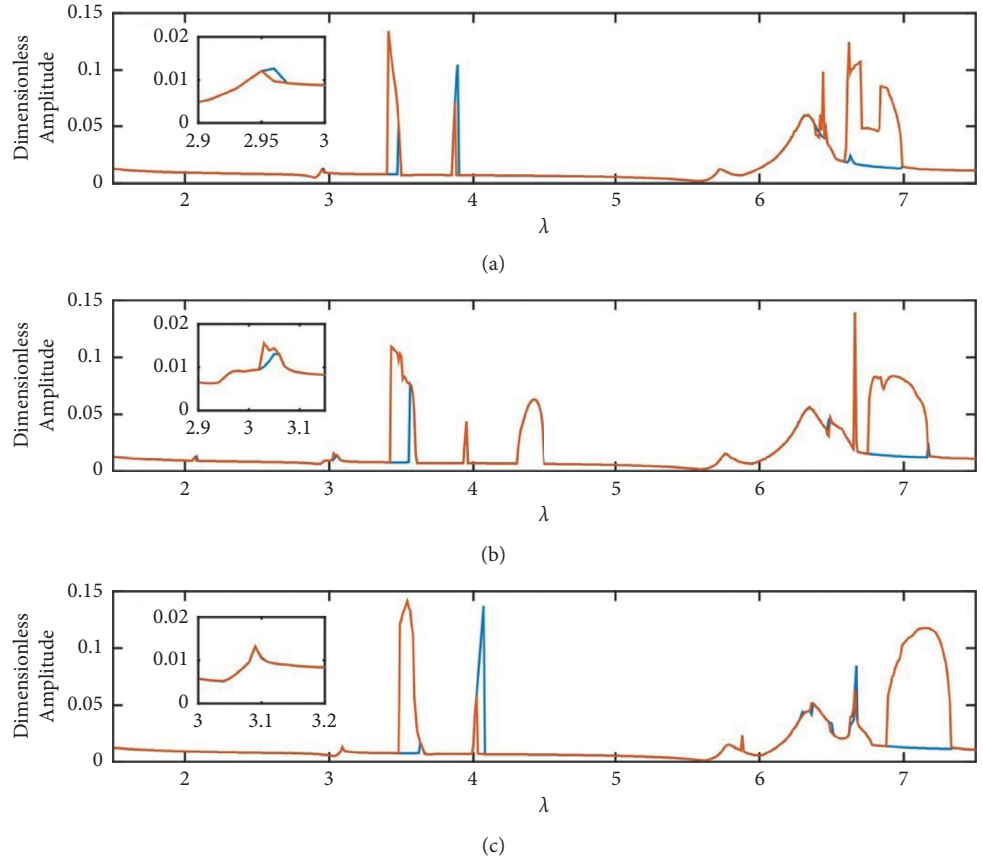

FIGURE 12: The amplitude-frequency curves of responses of disc in horizontal direction when (a) $N_b = 11$, (b) $N_b = 12$, and (c) $N_b = 13$ (blue line means run-up process and brown line means run-down process).

longer has the phenomenon of hysteresis jump. Comparing to Figure 12(c), it can be seen that the quasi-periodic motion is suppressed, and the amplitude-frequency response forms a wide range between the first-order main resonance region and the third-order main resonance region. For the journal, only in the second-order main resonance region can there be an obvious peak. At the same time, it should also be noted that the quasi-periodic motion of the third-order main resonance has not been eliminated but relatively suppressed. In general, the SFD has a more obvious suppression effect on the main resonance peak and quasi-periodic motion than other frequency components and can be used together with the bearing as means to reduce vibration and extend the life of the bearing.

Table 2: The quasi-periodic frequency with different numbers of balls.

Number of balls	Quasi-periodic frequency
$N_b = 11$	(1) $\lambda = 3.48$, $\lambda_f = 0.935$; (2) $\lambda = 3.87$, $\lambda_f = 0.968$; (3) $\lambda = 6.44$, $\lambda_f = 0.943$; (4) $\lambda = 6.9$, $\lambda_f = 0.927$
$N_b = 12$	(1) $\lambda = 3.06$, $\lambda_f = 0.971$; (2) $\lambda = 3.57$, $\lambda_f = 0.959$; (3) $\lambda = 3.95$, $\lambda_f = 0.964$; (4) $\lambda = 4.4$, $\lambda_f = 0.967$; (5) $\lambda = 6.56$, $\lambda_f = 3.043$; (6) $\lambda = 6.66$, $\lambda_f = 0.976$; (7) $\lambda = 6.91$, $\lambda_f = 0.928$
$N_b = 13$	(1) $\lambda = 3.08$, $\lambda_f = 0.978$; (2) $\lambda = 3.54$, $\lambda_f = 0.972$; (3) $\lambda = 4.07$, $\lambda_f = 0.993$; (4) $\lambda = 6.66$, $\lambda_f = 0.976$; (5) $\lambda = 7.15$, $\lambda_f = 0.96$

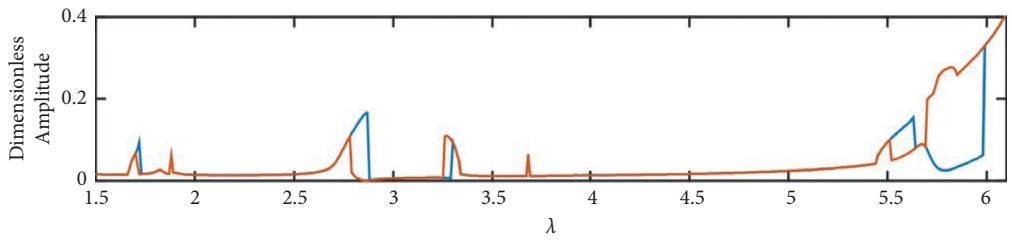

(a)

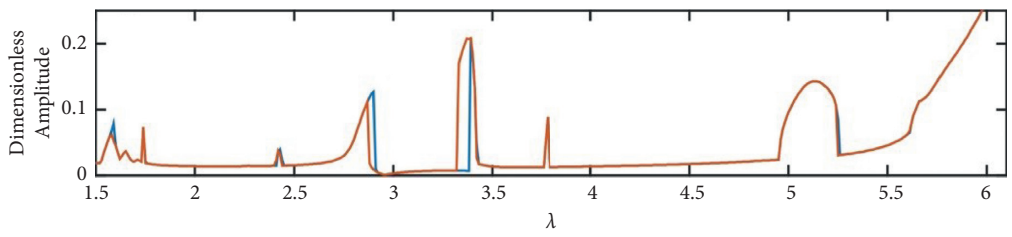

(b)

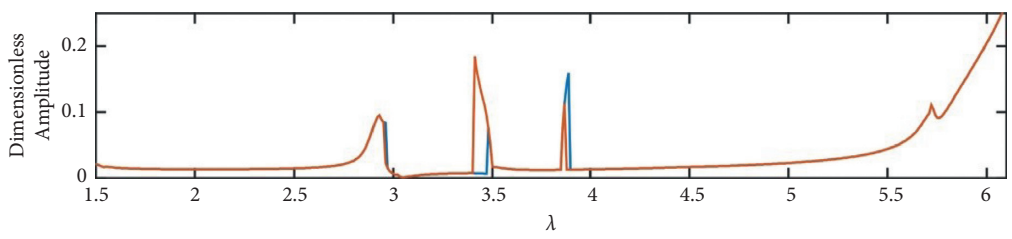

(c)

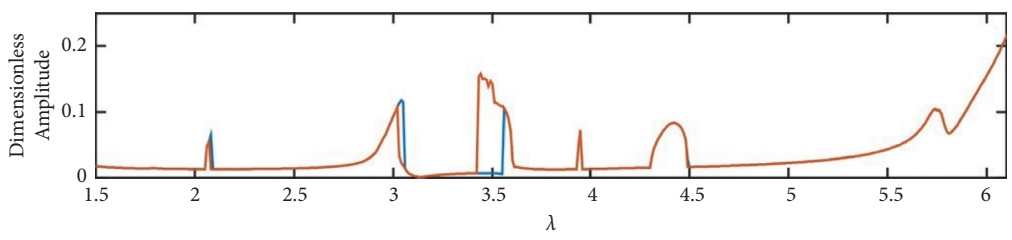

(d)

Figure 13: Continued.

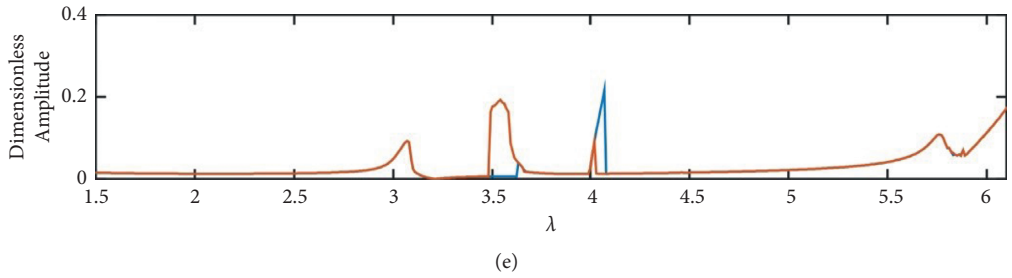

(e)

Figure 13: The amplitude-frequency curves of the left end journal in horizontal direction when (a) $N_b = 9$, (b) $N_b = 10$, (c) $N_b = 11$, (d) $N_b = 12$, and (e) $N_b = 13$ (blue line means run-up process and brown line means run-down process).

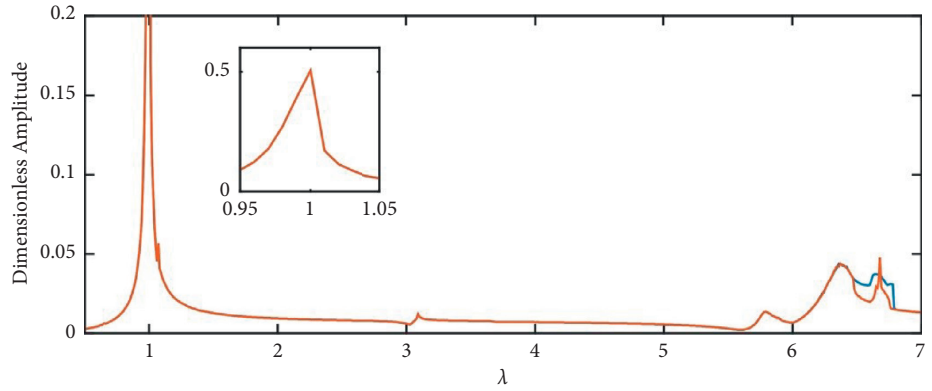

(a)

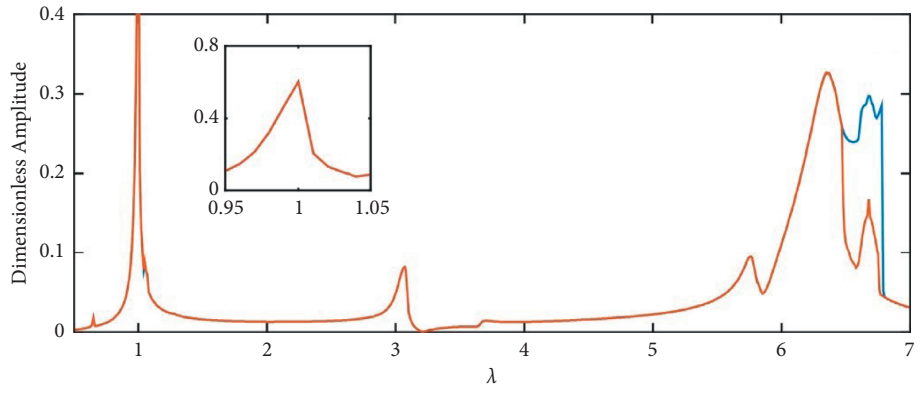

(b)

Figure 14: The amplitude-frequency curves of responses of (a) disc and (b) left-end journal in horizontal direction when $N_b = 13$ (blue line means run-up process and brown line means run-down process).

6. Conclusions

This paper studies the nonlinear response characteristics of an asymmetric rolling bearing supported rotor system with application of SFD in different resonance regions. The following conclusions can be drawn:

(1) In first three orders' prime resonance regions, the SFD suppresses the vibration significantly. Due to the nonlinearity introduced by the ball bearing, quasi-periodic solutions and jump behaviours still exist but with small amplitude.

(2) In VC frequency resonance region, the SFD almost has no damping effect because the amplitude of the response in VC frequency resonance case is small when no SFD is implemented. However, with the SFD, the soft and hard springs' coexisting characteristic would disappear when the number of balls increases.

(3) When the number of balls increases, the nonlinear responses, such as quasiperiodic motion and double period motion, still exist. The SFD suppresses the vibration of nonlinear components generally but

very little. However, with the SFD, the nonlinear behaviours and system stability would be affected by the number of balls.

All these characteristics can help us understand the dynamic behaviours of the ball bearing supported rotor systems with the application of the SFD, based on which the design basis of such kind of system can be given.

Appendix

$$\mathbf{C} = \begin{bmatrix} c_1 & 0 & 0 & -c_2 & \frac{-l_2c_1+c_2}{l} & 0 & -\frac{l_1c_1+c_2}{l} & 0 & 0 & 0 \\ 0 & c_1 & c_2 & 0 & 0 & \frac{-l_2c_1+c_2}{l} & 0 & -\frac{l_1c_1+c_2}{l} & 0 & 0 \\ 0 & c_3 & c_4 & 0 & 0 & \frac{-l_2c_3+c_4}{l} & 0 & -\frac{l_1c_3+c_4}{l} & 0 & 0 \\ -c_3 & 0 & 0 & c_4 & \frac{l_2c_3-c_4}{l} & 0 & \frac{l_1c_3+c_4}{l} & 0 & 0 & 0 \\ -\frac{l_2}{l}c_1 & 0 & 0 & \frac{l_2}{l}c_2 & \frac{l_2^2c_1-l_2c_2}{l^2} & 0 & \frac{l_1l_2c_1+l_2c_2}{l^2} & 0 & 0 & 0 \\ 0 & -\frac{l_2}{l}c_1 & -\frac{l_2}{l}c_2 & 0 & 0 & \frac{l_2^2c_1-l_2c_2}{l^2} & 0 & \frac{l_1l_2c_1+l_2c_2}{l^2} & 0 & 0 \\ -\frac{l_1}{l}c_1 & 0 & 0 & \frac{l_1}{l}c_2 & \frac{l_1l_2c_1-l_1c_2}{l^2} & 0 & \frac{l_1^2c_1+l_1c_2}{l^2} & 0 & 0 & 0 \\ 0 & -\frac{l_1}{l}c_1 & -\frac{l_1}{l}c_2 & 0 & 0 & \frac{l_1l_2c_1-l_1c_2}{l^2} & 0 & \frac{l_1^2c_1+l_1c_2}{l^2} & 0 & 0 \\ 0 & 0 & 0 & 0 & 0 & 0 & 0 & 0 & 0 & 0 \\ 0 & 0 & 0 & 0 & 0 & 0 & 0 & 0 & 0 & 0 \end{bmatrix},$$

$$\mathbf{K}=\begin{bmatrix}
k_{rr} & 0 & 0 & -k_{r\varphi} & \frac{-l_2k_{rr}+k_{r\varphi}}{l} & 0 & -\frac{l_1k_{rr}+k_{r\varphi}}{l} & 0 & 0 & 0\\
0 & k_{rr} & k_{r\varphi} & 0 & 0 & \frac{-l_2k_{rr}+k_{r\varphi}}{l} & 0 & -\frac{l_1k_{rr}+k_{r\varphi}}{l} & 0 & 0\\
0 & k_{\varphi r} & k_{\varphi\varphi} & 0 & 0 & \frac{-l_2k_{\varphi r}+k_{\varphi\varphi}}{l} & 0 & -\frac{l_1k_{\varphi r}+k_{\varphi\varphi}}{l} & 0 & 0\\
-k_{\varphi r} & 0 & 0 & k_{\varphi\varphi} & \frac{l_2k_{\varphi r}-k_{\varphi\varphi}}{l} & 0 & \frac{l_1k_{\varphi r}+k_{\varphi\varphi}}{l} & 0 & 0 & 0\\
-\frac{l_2}{l}k_{rr} & 0 & 0 & \frac{l_2}{l}k_{r\varphi} & \frac{l_2^2k_{rr}-l_2k_{r\varphi}}{l^2} & 0 & \frac{l_1l_2k_{rr}+l_2k_{r\varphi}}{l^2} & 0 & 0 & 0\\
0 & -\frac{l_2}{l}k_{rr} & -\frac{l_2}{l}k_{r\varphi} & 0 & 0 & \frac{l_2^2k_{rr}-l_2k_{r\varphi}}{l^2} & 0 & \frac{l_1l_2k_{rr}+l_2k_{r\varphi}}{l^2} & 0 & 0\\
-\frac{l_1}{l}k_{rr} & 0 & 0 & \frac{l_1}{l}k_{r\varphi} & \frac{l_1l_2k_{rr}-l_1k_{r\varphi}}{l^2} & 0 & \frac{l_1^2k_{rr}+l_1k_{r\varphi}}{l^2} & 0 & 0 & 0\\
0 & -\frac{l_1}{l}k_{rr} & -\frac{l_1}{l}k_{r\varphi} & 0 & 0 & \frac{l_1l_2k_{rr}-l_1k_{r\varphi}}{l^2} & 0 & \frac{l_1^2k_{rr}+l_1k_{r\varphi}}{l^2} & 0 & 0\\
0 & 0 & 0 & 0 & 0 & 0 & 0 & 0 & k_a & 0\\
0 & 0 & 0 & 0 & 0 & 0 & 0 & 0 & 0 & k_a
\end{bmatrix},\tag{A1}$$

$$\mathbf{G}=\begin{bmatrix}
0 & 0 & 0 & 0 & \cdots & 0\\
0 & 0 & 0 & 0 & \cdots & 0\\
0 & 0 & 0 & J_p & \cdots & 0\\
0 & 0 & -J_p & 0 & \cdots & 0\\
\vdots & \vdots & \vdots & \vdots & \ddots & 0\\
0 & 0 & 0 & 0 & \cdots & 0
\end{bmatrix}.$$

Data Availability

The data used to support the findings of the study are available from the corresponding author upon request.

Conflicts of Interest

On behalf of all authors, the corresponding author states that there are no conflicts of interest.

Acknowledgments

This work was supported by Shandong Provincial Natural Science Foundation, China (Grant nos. ZR2018BA021 and ZR2018QA005), the National Natural Science Foundation of China (Grant nos. 12102234, 11502161, and 11902184), and the China Postdoctoral Science Foundation (Grant no. 2017M622259).

References

[1] O. Schmitz, H. Klingels, and P. Kufner, "Aero engine concepts beyond 2030: Part 1–the steam injecting and recovering aero engine," *Journal of Engineering for Gas Turbines & Power*, vol. 143, no. 2, Article ID 021001, 2021.

[2] S. Kaiser, O. Schmitz, and H. Klingels, "Aero engine concepts beyond 2030: Part 2–the free-piston composite cycle engine," *Journal of Engineering for Gas Turbines & Power*, vol. 143, no. 2, Article ID 021002, 2021.

[3] O. Schmitz, S. Kaiser, H. Klingels et al., "Aero engine concepts beyond 2030: Part 3–experimental demonstration of technological feasibility," *Journal of Engineering for Gas Turbines & Power*, vol. 143, no. 2, Article ID 021003, 2021.

[4] M. Liang, T. Yan, J. Hu, and Z. Chen, "Effect of rolling bearing parameters on the nonlinear dynamics of offset rotor," *Proceedings of the Institution of Mechanical Engineers-Part C: Journal of Mechanical Engineering Science*, vol. 234, no. 15, pp. 2968–2978, 2020.

[5] R. Tomović, "A simplified mathematical model for the analysis of varying compliance vibrations of a rolling bearing," *Applied Sciences*, vol. 10, no. 2, p. 670, 2020.

[6] Y. Han, L. Yang, and T. Xu, "Analysis of static stiffness fluctuation in radially loaded ball and roller bearings," *Archive of Applied Mechanics*, vol. 91, no. 4, pp. 1757–1772, 2021.

[7] Z. Lu, S. Zhong, H. Chen, X. Wang, J. Han, and C. Wang, "Nonlinear response analysis for a dual-rotor system supported by ball bearing," *International Journal of Non-linear Mechanics*, vol. 128, Article ID 103627, 2021.

[8] T. G. Ghannad, C. Gastaldi, and T. M. Berruti, "Rolling bearing parametric excitation of a jeffcott rotor system," in *Turbo Expo: Power for Land, Sea, and Air*vol. 84218New York, NY, USA, American Society of Mechanical Engineers (ASME), 2020.

[9] Y. Cheng, K. Hu, J. Wu, H. Zhu, and X. Shao, "A convolutional neural network based degradation indicator construction and health prognosis using bidirectional long short-term memory network for rolling bearings," *Advanced Engineering Informatics*, vol. 48, Article ID 101247, 2021.

[10] H. Z. Chen, S. Zhong, Z. Y. Lu, Y. S. Chen, J. Han, and C. Wang, "Analysis on multi-mode nonlinear resonance and jump behavior of an asymmetric rolling bearing rotor," *Archive of Applied Mechanics*, vol. 91, pp. 2991–3009, 2021.

[11] K. Lu, Y. Jin, Y. Chen et al., "Review for order reduction based on proper orthogonal decomposition and outlooks of applications in mechanical systems," *Mechanical Systems and Signal Processing*, vol. 123, pp. 264–297, 2019.

[12] K. Lu, Y. Jin, P. Huang et al., "The applications of pod method in dual rotor-bearing systems with coupling misalignment," *Mechanical Systems and Signal Processing*, vol. 150, Article ID 107236, 2021.

[13] H. Cao, L. Niu, S. Xi, and X. Chen, "Mechanical model development of rolling bearing-rotor systems: a review," *Mechanical Systems and Signal Processing*, vol. 102, pp. 37–58, 2018.

[14] C. A. Fonseca, I. F. Santos, and H. I. Weber, "Influence of unbalance levels on nonlinear dynamics of a rotor-backup rolling bearing system," *Journal of Sound and Vibration*, vol. 394, pp. 482–496, 2017.

[15] H. Wang, X. Guan, G. Chen et al., "Characteristics analysis of rotor-rolling bearing coupled system with fit looseness fault and its verification," *Journal of Mechanical Science and Technology*, vol. 33, no. 1, pp. 29–40, 2019.

[16] Z. Luo, J. Wang, R. Tang, and D. Wang, "Research on vibration performance of the nonlinear combined support-flexible rotor system," *Nonlinear Dynamics*, vol. 98, no. 1, pp. 113–128, 2019.

[17] Y. Li, H. Cao, and K. Tang, "A general dynamic model coupled with efem and dbm of rolling bearing-rotor system," *Mechanical Systems and Signal Processing*, vol. 134, Article ID 106322, 2019.

[18] S. Fukata, E. H. Gad, T. Kondou, T. Ayabe, and H. Tamura, "On the radial vibration of ball bearings: cs," *Bulletin of JSME*, vol. 28, no. 239, pp. 899–904, 1985.

[19] B. Mevel and J. L. Guyader, "Routes to chaos in ball bearings," *Journal of Sound and Vibration*, vol. 162, no. 3, pp. 471–487, 1993.

[20] B. Mevel and J. L. Guyader, "Experiments on routes to chaos in ball bearings," *Journal of Sound and Vibration*, vol. 318, no. 3, pp. 549–564, 2008.

[21] W. Zhang, B. Han, X. Li, J. Sun, and Q. Ding, "Multi-objective system optimization method and experimental validation of a centralized squeeze film damper using a cell mapping method considering dynamic constraints," *Engineering Optimization*, vol. 53, no. 6, pp. 941–961, 2021.

[22] K. Shaik and B. K. Dutta, "Tuning criteria of nonlinear flexible rotor mounted on squeeze film damper using analytical approach," *Journal of Vibration Engineering & Technologies*, vol. 9, no. 2, pp. 325–339, 2021.

[23] K. Shaik and B. K. Dutta, "Stability analysis of horizontal symmetric flexible rotor mounted on hydrodynamic bearing and squeeze film damper using analytical approach," *Tribology International*, vol. 158, Article ID 106924, 2021.

[24] W. Zheng, S. Pei, Q. Zhang, and J. Hong, "Experimental and theoretical results of the performance of controllable clearance squeeze film damper on reducing the critical amplitude," *Tribology International*, 2021, inpress, Article ID 107155.

[25] T. Fan and K. Behdinan, "An analytical model for open-ended squeeze film damper with a circumferential central groove," *Proceedings of the Institution of Mechanical Engineers-Part J: Journal of Engineering Tribology*, vol. 235, no. 10, Article ID 1350650120987652, 2021.

[26] D. Shin, A. B. Palazzolo, and X. Tong, "Squeeze film damper suppression of thermal bow-morton effect instability," *Journal of Engineering for Gas Turbines & Power*, vol. 142, no. 12, Article ID 121013, 2020.

[27] X. Ma, H. Ma, H. Qin, X. Guo, C. Zhao, and M. Yu, "Nonlinear vibration response characteristics of a dual-rotor-bearing system with squeeze film damper," *Chinese Journal of Aeronautics*, vol. 34, pp. 128–147, 2021.

[28] X. Chen, X. Gan, and G. Ren, "Dynamic modeling and nonlinear analysis of a rotor system supported by squeeze film damper with variable static eccentricity under aircraft turning maneuver," *Journal of Sound and Vibration*, vol. 485, Article ID 115551, 2020.

[29] V. Iacobellis, K. Behdinan, D. Chan, and D. Beamish, "Experimental investigation of the effects of squeeze film damper design on highspeed rotor system," in *Turbo Expo: Power for Land, Sea, and Air*, vol. 84225, New York, NY, USA, American Society of Mechanical Engineers (ASME), 2020.

[30] W. Li, C. Braman, B. Hantz, M. Thorat, and B. Pettinato, "Squeeze film damper bearing with double-ended beam springs: Part ii–experimental validation," in *Turbo Expo: Power for Land, Sea, and Air*, vol. 84218, American Society of Mechanical Engineers (ASME), New York, NY, USA, 2020.